Restoration in 3D fluorescence microscopy

Saima Ben Hadj and Laure Blanc-Féraud

Work supported by ANR DIAMOND

Morphème Research Group

November 29, 2011

Outline

Introduction

For **space-invariant** blurred images, the following model is used:

$$g(u) = \sum_{t \in \mathcal{R}} \left[h(u-t) . f(t) \right] \tag{1}$$

$\Longrightarrow$ Computations are fast using **Fast Fourier Transform**.

For **space-variant** blurred images, the model is expressed as follows:

$$g(u) = \sum_{t \in \mathcal{R}} \left[h(u,t) . f(t) \right] \tag{2}$$

$\Longrightarrow$ Computations are very long.

Space-variant blur due to light refraction phenomenon

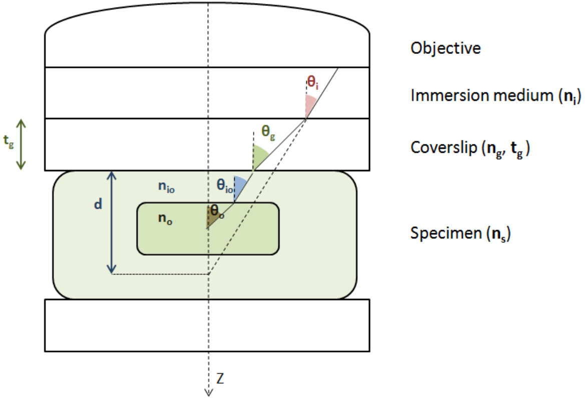

Figure 1: Ray deviation due to refractive index mismatch between mediums composing the system and the specimen.

PSF variation with depth in CLSM system

Maximum intensity projection onto (X,Y)

Maximum intensity projection onto (X,Z)

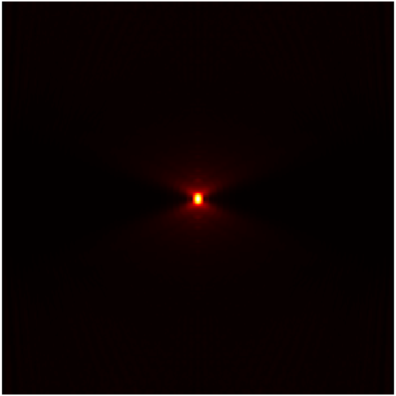

Space-variant blur modeling

SV blur models can be divided into two classes:

Class 1: Nagy et al, 1998

- Degradation model:

$$g(u) = \sum_{1 \leq i \leq D} \psi_i(u) \,.\, (h_i * f)(u) \quad (3)$$

- Associated SV PSF:

$$\widetilde{h}(u,t) = \sum_{1 \leq i \leq D} \psi_i(u) \,.\, h_i(u-t) \quad (4)$$

Class 2: Hirsch et al., 2010

- Degradation model:

$$g(u) = \sum_{1 \leq i \leq D} h_i * (\psi_i . f)(u) \quad (5)$$

- Associated SV PSF:

$$\widetilde{h}(u,t) = \sum_{1 \leq i \leq D} \psi_i(t) \,.\, h_i(u-t) \quad (6)$$

$\Longrightarrow$ What is the most accurate model?

Exemple of weighting functions

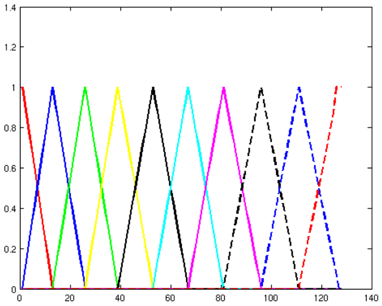

Figure 2: triangular weighting functions

Blur model assessment and selection

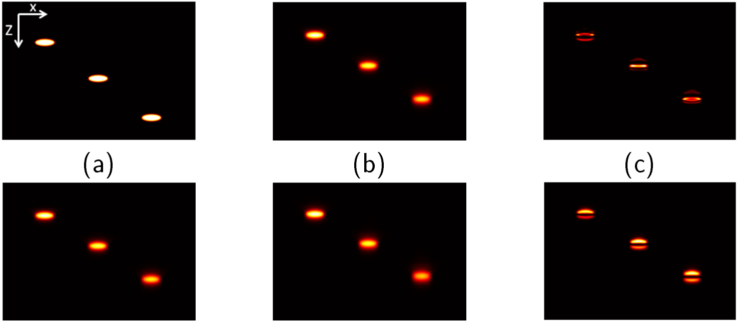

(a) (b) (c) (d) (e) (f)

Figure 3: (a) Object, (b) observation according to Nagy et al., (c) error between the theoretical blurred image and simulation according to Nagy et al., (d) theoretical blurred image, (e) observation according to Hirsch et al., (f) error between the theoretical blurred image and simulation according to Hirsch et al.

Blur model assessment and selection

	Nagy et al.	Hirsch et al.
RSE (%)	0.02	27.64
Correlation coef.	0.99	0.87
SSIM	0.99	0.94

Table 1: Comparing approximate space variant blur models to the theoretical blur model.

Restoration in a framework of Poisson noise: method

- Degradation model under Poisson noise assumption: $g = \mathcal{P}\left(\widetilde{H}(f)\right)$.
- Image restoration by minimizing the following energy function:

$$J_1(f) = \left[\sum_u \widetilde{H}(f)(u) - g(u)\log\left(\widetilde{H}(f)(u)\right)\right] + \alpha\|\nabla f\|_1 \qquad (7)$$

- A modified version of the RLTV iteration is the following:

$$f^{k+1} = \frac{f^k}{\widetilde{H}^*(1) - \alpha div\left(\frac{\nabla f^k}{|\nabla f^k|}\right)}\widetilde{H}^*\left(\frac{g}{\widetilde{H}(f^k)}\right) \qquad (8)$$

where $\widetilde{H}(.) = \sum_{1\leq i\leq D} \psi_i.H_i(.)$, and $H_i(.) = h_i * .$ and

$\widetilde{H}^*(f) = \sum_{1\leq i\leq D} H_i^*(\psi_i.f)$ is adjoint of $\widetilde{H}$ with H_i^* the adjoint of H_i.

Restoration in a framework of Poisson noise: result

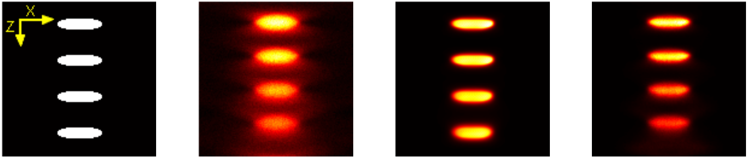

(a) (b) (c) (d)

Figure 4: Restoration under Poisson noise condition: (X,Z) slices of (a) the object, (b) the observation, (c) the restoration using $\widetilde{H}$, (d) the restoration using a space-invariant PSF.

Comparing the proposed method to EMMA

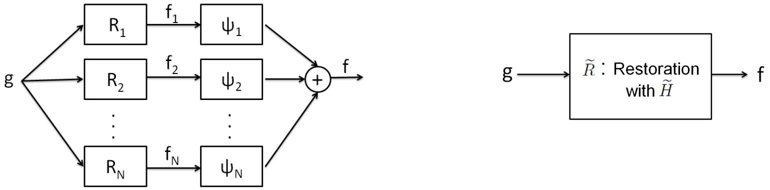

(a) EMMA.

(b) Restoration with a SV PSF.

Figure 5: (a) SV restoration using EMMA. R_i, $i = 1, ..., N$ refers to the restoration with the SI convolution kernel h_i, and (b) Restoration using the proposed space-variant blur function $\widetilde{H}$.

Comparing the proposed method to EMMA

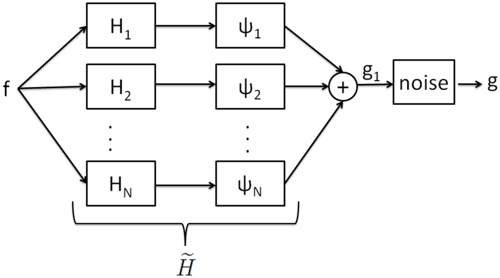

Figure 6: The proposed space-variant blur modeling.

Restoration in a framework of Poisson noise: result

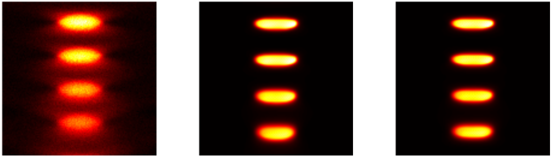

(a) (b) (c)

Figure 7: Restoration under Poisson noise condition: (X,Z) slices of (a) the observation, (c) the restoration using EMMA, (d) the restoration using $\widetilde{H}$.

Restoration in a framework of Poisson noise: result

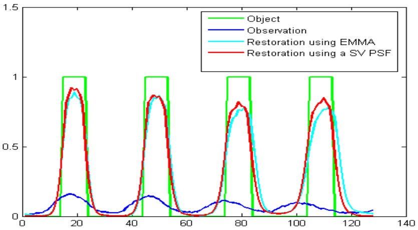

Figure 8: Intensity profiles along the z-axis: the green plot corresponds to the object, the blue one corresponds to the observation, the cyan one corresponds to the restoration using EMMA and the red plot corresponds to the restoration with $\widetilde{H}$. Restorations are based on the RLTV algorithm.

Restoration in a framework of Gaussian noise: method

- Degradation model under Gaussian noise assumption:
  $g = \left(\widetilde{H}(f)\right) + n.$
- Image restoration by minimizing the following energy function:

$$J_2(f) = \left\| \widetilde{H}(f) - g \right\|_2^2 + \alpha \left\| \nabla f \right\|_1 \tag{9}$$

- We use a fast minimization method based on a domain decomposition technique, developed by Fornasier et al., 2009. Using this method and a small intersection between 2 sub-domains, one can gain about 30% of the computing time spent by ADM method.

Fornasier et al method

- Split the image domain Ω into 2 overlapping sub-domains such that $\Omega = \Omega_1 \cup \Omega_2$ and $\Omega_1 \cap \Omega_2 \neq \emptyset$.
- The solution f in the whole domain Ω can be split as follows:

$$f(u) = \begin{cases} f_1(u) & if\ u \in \Omega_1 \setminus \Omega_2 \\ f_1(u) + f_2(u) & if\ u \in \Omega_1 \cap \Omega_2 \\ f_2(u) & if\ u \in \Omega_2 \setminus \Omega_1 \end{cases} \quad (10)$$

- Energy minimization is performed in each sub-domain separately:

$$\begin{cases} f_1^* = Arg \underset{support(f_1) \subset \Omega_1 / f_1|_{\Gamma_1} = 0}{Min} J(f_1 + f_2) \\ f_2^* = Arg \underset{support(f_2) \subset \Omega_2 / f_2|_{\Gamma_2} = 0}{Min} J(f_1 + f_2) \end{cases} \quad (11)$$

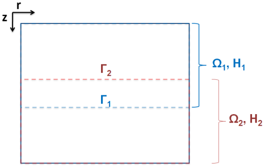

Figure 9: Overlapping domain decomposition.

Local minimization

- Local minimization: $f_1^* = Arg \underset{support(f_1)\subset\Omega_1 / f_1|_{\Gamma_1}=0}{Min} J(f_1 + f_2)$ is performed using Lagrange multiplier scheme.
- Minimize an auxiliary function of $J(.)$ in order to use the following theorem.

Theorem: oblique thresholding

The following two statements are equivalent:

1. $f_1^* = Arg \underset{support(f_1)\subset\Omega_1 / f_1|_{\Gamma_1}=0}{Min} \|f_1 - z_1\|_2^2 + 2\alpha \|\nabla (f_1+f_2) | (\Omega_1)\|_1$,
2. $\exists \eta$ with $support(\eta) = \Gamma_1$ such that:

$$f_1^* = (I - P_{\alpha K})(z_1 + f_2 - \eta) - f_2 \text{ and } f_1^*|_{\Gamma_1} = 0$$

with $P_{\alpha \mathrm{K}}(.)$ the orthogonal projection onto the closed convex set K related to the total variation term.

Convergence of the proposed method

Two necessary convergence conditions are verified in [Ben Hadj and Blanc-Féraud, 2011]:

1. The coercivity of the energy functional $J(.)$ for the space varying operator $\widetilde{H}$ i.e. $J(f) \rightarrow +\infty$ as $\|f\| \rightarrow +\infty$,
2. $\left\|\widetilde{H}\right\|_2 \leq 1$, a necessary condition for characterizing the sequence $\left(f^{(n)}\right)_{n\in\mathbb{N}}$ produced during the iterations of the proposed algorithm (for example, $\lim_{n\rightarrow\infty} \left\|f^{(n+1)} - f^{(n)}\right\|_2 = 0$).

Restoration in a framework of Gaussian noise: result

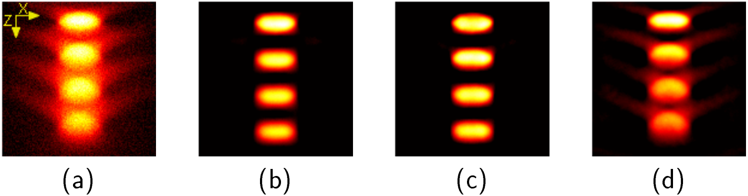

Figure 10: Restoration under Gaussian noise condition: (X,Z) slices of (a) the observation, (b) the restoration using EMMA, (c) the restoration using $\widetilde{H}$, and (d) restoration with a SI PSF.

Restoration in a framework of Gaussian noise: result

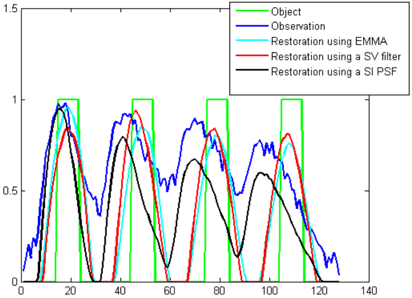

Figure 11: Intensity profiles along the z-axis: the green plot corresponds to the object, the blue one corresponds to the observation, the cyan one corresponds to the restoration using EMMA, the red one corresponds to the restoration with $\widetilde{H}$ and the black one corresponds to the restoration with a SI PSF.

Comparing the proposed method to EMMA

	EMMA method		Restoration with $\widetilde{H}$	
Noise	Poisson	Gauss	Poisson	Gauss
RSE mean (%)	24.21	39.7	22.49	39.54
SSIM mean	0.83	0.73	0.85	0.74
Mean time (mn)	20	22	9	6

Table 2: Comparing the proposed space-variant restoration method to EMMA.

Conclusion (1)

Summary

- Consideration of a blur modeled by a convex combination of convolutions with space-invariant PSF.
- Inversion of this model using two restoration methods under Poisson and Gaussian noise conditions.
- Comparison with EMMA method.
- Validation on simulated bead images of CLSM and WFM.

Future works

- Test on real data.
- Exploration of the blind deconvolution case.
- Exploitation of the TDM data for blind deconvolution of CLSM images.

Reconstruction of the TDM data

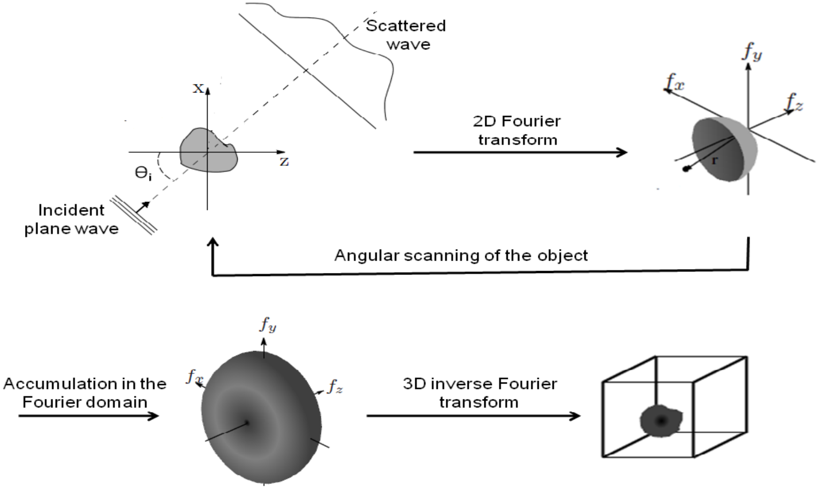

TDM data versus CLSM data

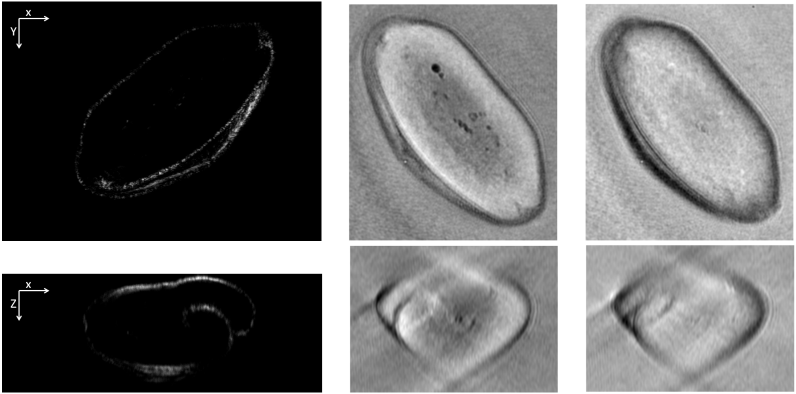

Figure 12: The first column corresponds to the CLSM data, the second column corresponds to imaginary part of the TDM data and the third column corresponds to the real part of the TDM data.

Frequency representation of the TDM pollen image

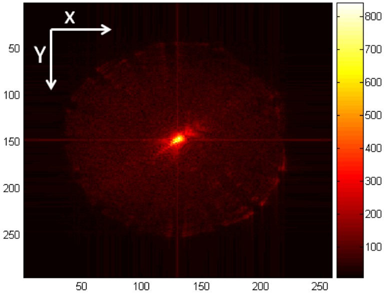

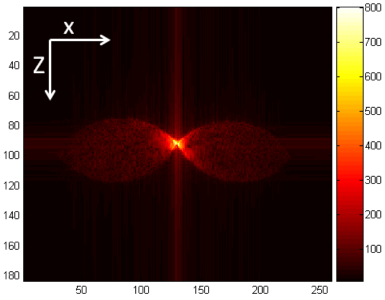

Figure 13: (a) Radial and (b) axial slices of the Fourier transform module of the pollen image.

Using TDM data for CLSM image restoration

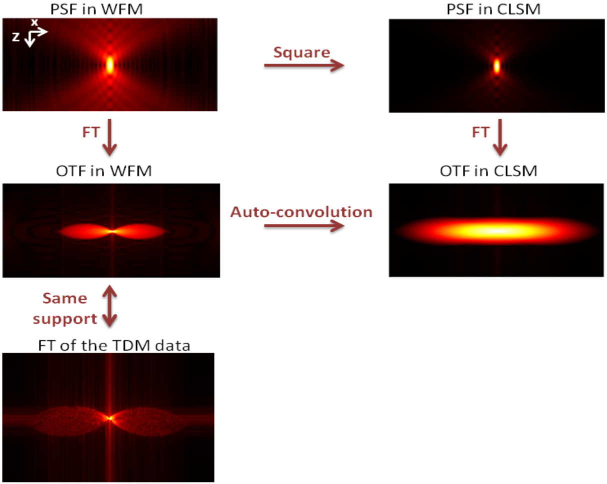

Conclusion (2)

Future works

- Exploit the TDM data in order to regularize the support of the OTF in CLSM.